



HAL
open science

Coupling LiDAR and structural models to improve the estimation of aboveground woody biomass

Rémi Vezy, Mathilde Millan, Alexis Bonnet, Jean Dauzat

► **To cite this version:**

Rémi Vezy, Mathilde Millan, Alexis Bonnet, Jean Dauzat. Coupling LiDAR and structural models to improve the estimation of aboveground woody biomass. 2022. hal-03838571

HAL Id: hal-03838571

<https://hal.science/hal-03838571>

Preprint submitted on 3 Nov 2022

HAL is a multi-disciplinary open access archive for the deposit and dissemination of scientific research documents, whether they are published or not. The documents may come from teaching and research institutions in France or abroad, or from public or private research centers.

L'archive ouverte pluridisciplinaire **HAL**, est destinée au dépôt et à la diffusion de documents scientifiques de niveau recherche, publiés ou non, émanant des établissements d'enseignement et de recherche français ou étrangers, des laboratoires publics ou privés.

Coupling LiDAR and structural models to improve the estimation of aboveground woody biomass

Rémi Vezy^{a,b,*}, Mathilde Millan^{a,b}, Alexis Bonnet^{a,b}, Jean Dauzat^{a,b}

^aCIRAD, UMR AMAP, F-34398 Montpellier, France.

^bAMAP, Univ Montpellier, CIRAD, CNRS, INRAE, IRD, Montpellier, France.

*Corresponding author. Email address: remi.vezy@cirad.fr (Rémi Vezy).

Abstract

LiDAR is a promising tool for fast and accurate measurements of trees. There are several approaches to estimate aboveground woody biomass using LiDAR point clouds. One of the most widely used method consists in fitting geometric primitives (*e.g.* cylinders) to the point cloud, thereby reconstructing both the geometry and topology of the tree. However, current algorithms are not suited for accurate estimation of the biomass of finer branches, because of the unreliable point dispersions from the movements induced by wind, occlusion in the upper canopy, or the relatively large laser footprint compared to the structure diameter.

We propose a new method that couples point cloud-based reconstructions and structural models to estimate accurately the aboveground woody biomass of trees, including finer branches. The model was trained using branch samples from the trees, and accurately predicted the biomass with 1.6% nRMSE at the segment scale from a k-fold cross-validation. It also gave satisfactory results when up-scaled to the branch level with a significantly lower error (13% nRMSE) and bias (-5%) compared to fitting cylinders to the point cloud (nRMSE: 92%), or using the pipe model theory (nRMSE: 31%).

The model was then applied to the whole-tree scale, and showed that the sampled trees had more than 1.7km of structures in average, and that 96% of that length was coming from the twigs (*i.e.* <5 cm diameter). Our results showed that neglecting twigs lead to a significant underestimation of tree aboveground woody biomass (-21%) in our study case.

The structural model approach is promising for unbiased large-scale estimations, and could be used as a new way for accurate estimation of the standing biomass without the need for tree cutting.

Keywords: *tree; walnut; agroforestry; laser; architecture; allometry; topology; Multi-Scale Tree*

Graph

32 **1. Introduction**

33 The three-dimensional reconstruction of plants with high accuracy is crucial for many fields
34 (Calders et al., 2015). For example, it is used to precisely estimate the carbon stock of large
35 populations of trees in forests and agroforestry systems, a key information to better understand
36 the functioning of the terrestrial carbon cycle. It is also frequently used to estimate the
37 aboveground woody biomass for logging, or to parameterize functional-structural plant models
38 to simulate radiation interception, fluxes of carbon, water and nutrients, biomass allocation, or
39 even assessing and optimizing innovative planting designs (Perez et al., 2018).

40 LiDAR is a promising tool for fast and precise acquisition of data at large scale (Dassot et al.,
41 2011; Calders et al., 2020). There are several algorithms for the reconstruction of tree topology
42 and geometry from LiDAR point clouds (Thies et al., 2004; Calders et al., 2020), and one of the
43 most successful attempt to date is by generating Quantitative Structural Models (QSM) using *e.g.*
44 TreeQSM (Raumonen et al., 2013) to adjust cylinders to the point cloud. However, this method
45 tends to overestimate the volumes of the branches towards the top of the canopy (Wilkes et al.,
46 2017) and the smaller branches (Demol et al., 2022). This is mainly due to occlusion, wind effect,
47 co-registration errors and laser footprint that becomes large compared to the diameter of
48 branches smaller than 2 cm (Abegg et al., 2021). Some attempts have been made to correct for
49 the beam divergence issue (Wilkes et al., 2021), but correcting for wind effect, occlusion or
50 under-sampling is more difficult.

51 New approaches are emerging to reduce such errors by coupling LiDAR data with structural
52 models. For example Hu et al. (2021) report that TreeQSM made inaccurate individual branch
53 extraction, and used four consecutive empirical models instead to estimate the positions of the
54 whorl along the trunk, the number of branches in the whorls, the branch basal area and finally
55 their biomass. Unfortunately, this approach needs a consequent database to parameterize each
56 model, and with the assumption that the reconstruction of the branches is incorrect, the method

57 uses only a small portion of the rich LiDAR data (*i.e.* points of the main axes), neglecting valuable
58 information such as actual number of axis, their lengths and the tree topology.

59 We agree that coupling LiDAR data, 3D reconstruction software and structural models is
60 promising and can reduce the sensitivity to occlusion, co-registration errors and laser footprint.
61 However, we argue that this method can be further improved by exploiting the full extent of the
62 information from the LiDAR point clouds, by extracting more features from the tree such as
63 lengths, topology and spatial arrangements of all the structures, including small branches.

64 In this study, we present a new approach for the estimation of the aboveground woody biomass
65 with LiDAR. The approach uses 1/ the Plantscan3d software (see 2.3.1) to finely reconstruct the
66 tree topology and geometry; 2/ a statistical model based on tree structural features (*i.e.*
67 allometric relationships) to estimate the cross-sectional area of the structures; and 3/ the
68 volumes of the structures and the wood density for the estimation of the aboveground woody
69 biomass.

70 The structural model is then applied to the whole trees to compute general features and visually
71 assess its performance when upscaling.

72 **2. Material and methods**

73 **2.1. Experimental site**

74 The experimental site is located in Roumassouze in the South of France (44°03'29.6 "N 4°06'43.5
75 "E). It is an agroforestry system based on hybrid walnut trees (*Juglans regia* × *J. nigra*)
76 associated with a diversified and organic vegetable production. This experiment was conducted
77 on a plot of three hectares planted in 1996 with a tree spacing of 10 m x 10 m (*i.e.* 100 trees ha⁻¹).
78 The trees were thinned at 90 trees ha⁻¹ in 2011, and lightly pruned in 2015 by removing the
79 lower branches (*c.a.* 1.9 kg dry mass tree⁻¹). The trees were free growing since then.

80

81 **2.2. Measurements**

82 **2.2.1. LiDAR acquisition**

83 Measurements were conducted on three walnut trees from the experimental site. Two branches
84 per tree were identified, one close to the ground and the other upper in the tree canopy.
85 Reflective tape was placed at the branch basis for identification in the point cloud and for further
86 measurements.

87 The three trees were scanned prior to destructive sampling and without leaves on March 2021
88 with a Riegl VZ-400 LiDAR scanner (RIEGL Laser Measurement Systems GmbH). Twenty
89 positions were scanned both in upright and tilted positions. The scans were then co-registered
90 with RiScan Pro 2.11.3 using the reflective targets positioned in the field.

91 **2.2.2. Destructive method**

92 The six branches identified by reflective tape were cut at their basis. Measurements of topology,
93 wood density, woody biomass and dimensions were performed. The branches were 5.5 m long
94 in average, with a total of *c.a.* 390 m of segments measured by hand.

95 The topology was encoded for each branch using the Multi-scale Tree Graph (MTG) format
96 (Godin and Caraglio, 1998), and described using three complementary scales: the branch, the
97 axis and the segments. The axis (A) were defined as the succession of segments produced by the
98 apical meristem, and the segments (S) as the wood portion between two ramifications (Figure
99 1).

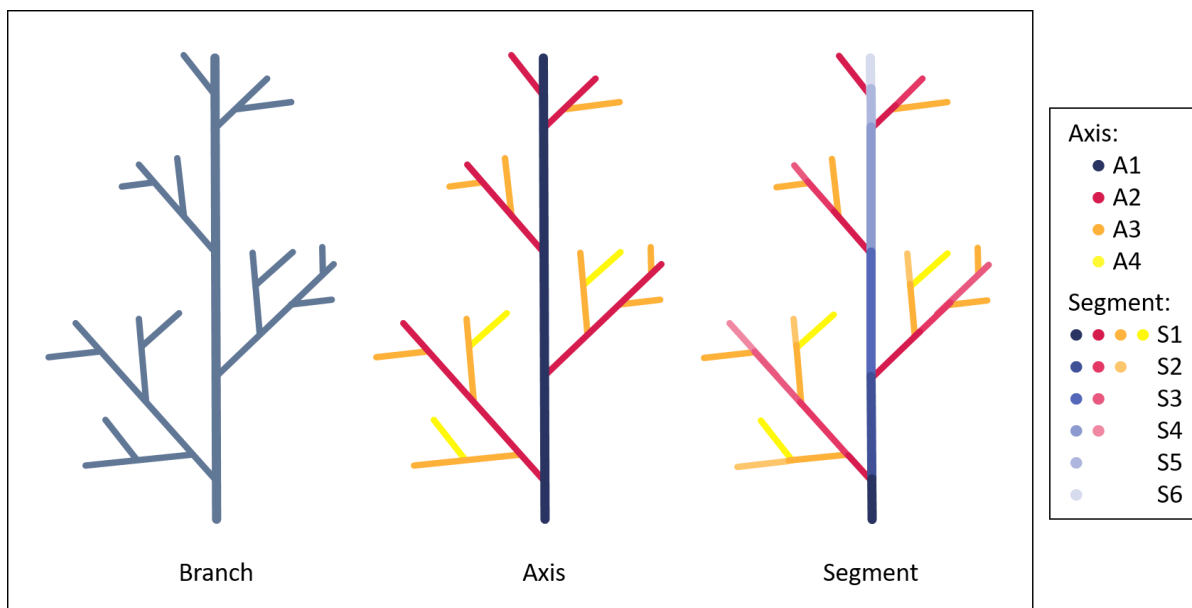
100 The branching order of each axis were determined considering the first (*i.e.* principal) axis as an
101 axis of order one by convention. Then the branching order recursively increased for each
102 branching point. A total of 5287 topological data point were collected in the six branches.

103 The fresh and dry density of the branches were estimated from the average value of ten sections
104 evenly sampled along the principal axis (A1) for each branch. Fresh biomass was measured for
105 the whole branch and for each second order axis (A2) including the structures of lower order.

106 The biomass of the first order axis (A1) was then calculated as the total branch biomass minus
107 the cumulated biomass of the second order axis, unless there are missing measurements for A2,
108 in which case it was not used for comparison (*i.e.* branches 13-h and 13-l).

109 Radius was measured at the mid-point of each segment with two perpendicular orientations
110 using digital calipers. Segment length was also recorded with a measuring tape. The volume of
111 each segment was then computed using the radius and length considering segments as cylinders.
112 The biomass of each segment was estimated using the volume and average wood density. This
113 method was found sufficient when comparing the computed biomass of the axis with the actual
114 measurement with a scale (see Figure A 1).

115 All measurements were encoded into the MTG as attributes.



117 **Figure 1: Schematic representation of the topological encoding of a branch at three scales: the branch, the**
118 **axis, and the segment. The axes are defined as the succession of segments produced by the apical meristem,**
119 **and the segments as the wood portion between two ramifications, including the portion of the ramification at**
120 **the apex. Axes are numbered by branching order, segments by acropetal index on the axis.**

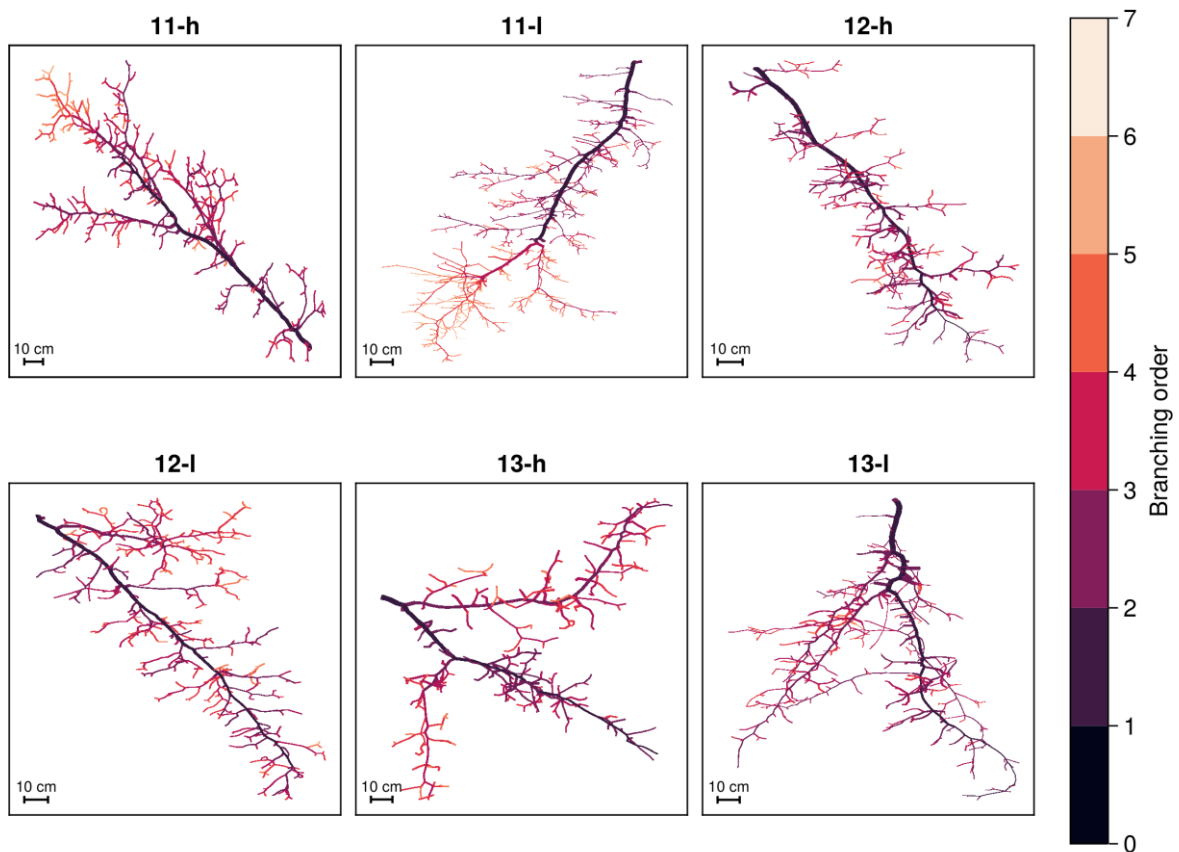
121 **2.3.Reconstruction**

122 **2.3.1. Plantscan3D**

123 The plantscan3D software (<https://github.com/openalea/plantscan3d>) was used for the
124 reconstruction of the topology, length and diameter of the branches and the whole-trees from

125 the LiDAR point clouds (Figure 2). The topology was reconstructed using the skeletonization
126 algorithm from Xu et al. (2007). This algorithm first builds a Riemannian graph by connecting
127 the k closest neighbors points. The graph is then segmented into clusters of points using the
128 distance from a root point, and the center of each cluster is finally used as nodes for the tree
129 skeleton (Boudon et al., 2014). Light manual corrections were performed to ease the comparison
130 with the destructive method, for example by correcting the branching type between nodes (*i.e.*
131 branch or follow), or the position of the base of a branch when two ramifications are branching
132 close to each other. The radius of each segment was estimated using the average point distance
133 algorithm that fits a cylinder to the neighbor points.

134 The resulting topology was exported as an MTG file, and further processed with the
135 MultiScaleTreeGraph.jl package (Vezy, 2022).



136

137 **Figure 2. Fully automated reconstruction of the topology and geometry of the six branches using Plantscan3d.**
138 **The branch is named after the tree index and the position in the tree: high (h) or low (l).**

139 **2.3.2. Pipe model theory (PMT)**

140 The pipe model derives from a simple and intuitive theory that states that each leaf in a plant is
141 connected to the stem base via a pipe with a constant cross-sectional area (Shinozaki et al.,
142 1964; Valentine, 1985). One of the property of the theory is that “*the conductive surface area of a*
143 *stem at a given height is equal to the cumulative basal area of its daughter axes above that height*”
144 (Lehnebach et al., 2018). In this paper, we used a simplified formulation earlier defined by
145 Leonardo da Vinci that replaces the conductive cross-sectional area by the total cross-sectional
146 area (CSA). This theory is over-simplified but simpler to use with LiDAR data where only the CSA
147 is available. In practice, we used this method to compute the diameters of all segments in a
148 branch or tree starting from the basal segment, and iteratively partitioning the CSA to its
149 children segments, weighted by the total number of terminal segments in the child subtree. This
150 model was applied on the MTG of the branches to estimate the diameters of all segments using
151 the radius of the first segment estimated by plantscan3D as a starting point.

152 **2.3.3. Structural model**

153 The new method presented in this paper uses Plantscan3d to reconstruct the skeleton of a
154 branch or tree, and a model based on structural traits to compute the CSA of the structures. To
155 do so, a statistical linear model is defined and fitted using manual measurements at segment and
156 axis scale only using features we can also derive from LiDAR point clouds such as:

- 157 - CSA estimated using the PMT
- 158 - Total length of the subtree
- 159 - Branching order
- 160 - Relative acropetal position of the segment (*i.e.* from the tip) on its axis
- 161 - Number of segments in the subtree
- 162 - Number of terminal segments

163 - Number of segments on the axis

164 - Length of the axis

165 The first step for building such model is to identify which candidate variable explains the
166 variability in the cross-sectional area of the segments. The p-value of each variable selected for
167 the model was controlled for its significance, and all variables with a p-value lower than 0.05
168 was discarded from the model.

169 The second step consisted in the evaluation of the robustness of the model using a k-fold cross-
170 validation ($k = 10$). The model is trained and evaluated k-times on sub-samples of the data,
171 which helps computing the out-of-sample nRMSE.

172 In the third step, we trained the model using the whole dataset to compute its parameters for
173 use in the reconstructions, and evaluate its accuracy with the in-sample nRMSE.

174 Finally, the last step was to apply the model on the MTG obtained from the Plantscan3d
175 reconstruction to predict the cross-sectional area of any segment in the tree or branch.

176 **2.4. Merging manual and LiDAR-based reconstructions**

177 Matching the results of the manual measurements and the model reconstructions is not trivial
178 because a little difference in *e.g.* the definition of the main axis or in the position of the base of a
179 branch can lead to very different MTG outputs. Furthermore, the manual measurements were
180 performed months after the LiDAR acquisition, which eventually lead to missing broken
181 structures in the manual measurements.

182 To alleviate these issues, the MTG of both methods were compared manually, and all axes that
183 could be recognized in both were identified with a unique identifier. In this paper, all
184 comparisons between manual and LiDAR-derived measurements are done using these axes.

185 **2.5. Data and code availability**

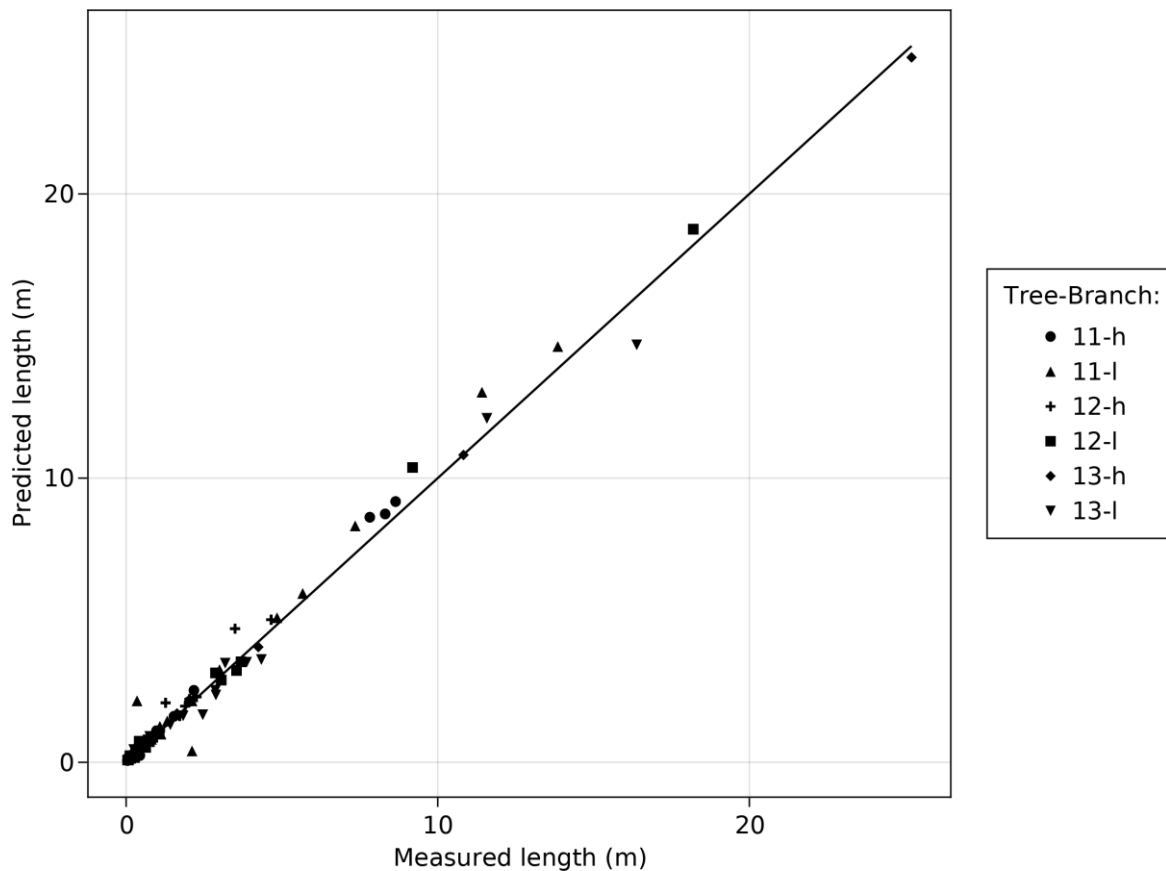
186 The code developed in this study for analysis, modelling, 3D reconstruction, statistics and figures
187 is available on a GitHub repository (https://github.com/VEZY/Biomass_evaluation_LiDAR) and
188 fully archived on Zenodo (Vezy et al., 2022).

189 3. Results

190 3.1. Axis length

191 The axes lengths estimated by Plantscan3d using the LiDAR point clouds were compared to the
192 destructive measurements. The comparison is performed using the total length of all segments
193 forming an axis. As expected, the lengths estimated by Plantscan3d were close to the manual
194 measurements, with only 1% nRMSE and a bias close to zero (0.2%), which indicates that the
195 error is not cumulative (Figure 3).

196 The estimation is correct for all the range of axis lengths whatever the number of segments, and
197 the error is conservative between trees, which shows the genericity of the method.



198

199 **Figure 3. Measured (x-axis) and predicted (y-axis) length at axis scale. Normalized Root Mean Squared Error**
 200 **(nRMSE): 1%; Modelling Efficiency (EF): 0.99; Normalized Bias: 0.2%. The branch is named after the tree**
 201 **index and the position in the tree: high (h) or low (l).**

202

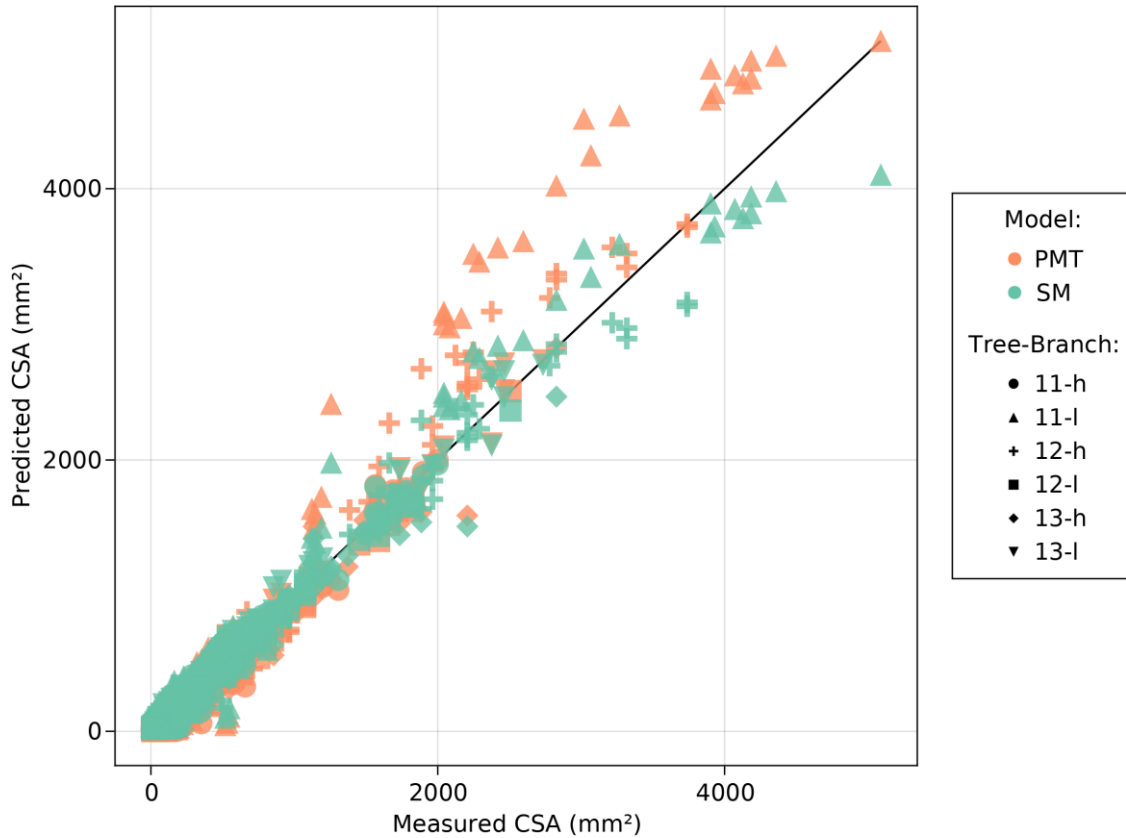
203 **3.2. Model training and evaluation**

204 The final model had six variables, and obtained an nRMSE of 1.58% \pm 0.4 on the cross-validation
 205 evaluation, and 1.4% when trained on the full dataset. Two variables did not explain
 206 significantly the variability in the cross-sectional area and were excluded from the model: the
 207 number of segments on the axis and the length of the axis.

208 **Table 1. Linear model fitting summary (i.e. structural model). Coef.: estimate of the coefficients; Std. Error:**
 209 **standard error; t: t-value; Pr(>|t|): p-value; Lower/Upper 95 %: lower and upper values of the confidence**
 210 **interval; CSA: cross-sectional area; PMT: pipe model theory.**

Variable	Coef.	Std. Error	t	Pr(> t)	Lower 95%	Upper 95%
CSA from the PMT	0.52	0.015	34.34	<1e-99	0.49	0.55
Path length of the subtree	0.015	0.0007	21.35	<1e-94	0.0139	0.0167
Branching order	6.38	1.28	5.00	<1e-06	3.88	8.89
Segment index on axis	10.94	0.41	26.65	<1e-99	10.13	11.74
N of terminal segments	-10.14	2.13	-4.77	<1e-05	-14.31	-5.97
N segments on the subtree	4.47	1.05	4.2	<1e-04	2.40	6.54

211 As expected, the CSA computed using the PMT was the variable with the highest importance (t-
 212 value= 34, Table 1), followed by the index of the segment on the axis (t-value= 27), and the total
 213 length of the subtree (t-value= 21). Although significant, the three other variables had a lower
 214 importance ($|t\text{-value}| \leq 5$) in the model.



215

216 **Figure 4. Measured (x-axis) and predicted (y-axis) cross-sectional area (CSA) at segment scale by the**
 217 **structural model (SM, this study), or the pipe model theory (PMT). The branch is named after the tree index**
 218 **and the position in the tree: high (h) or low (l).**

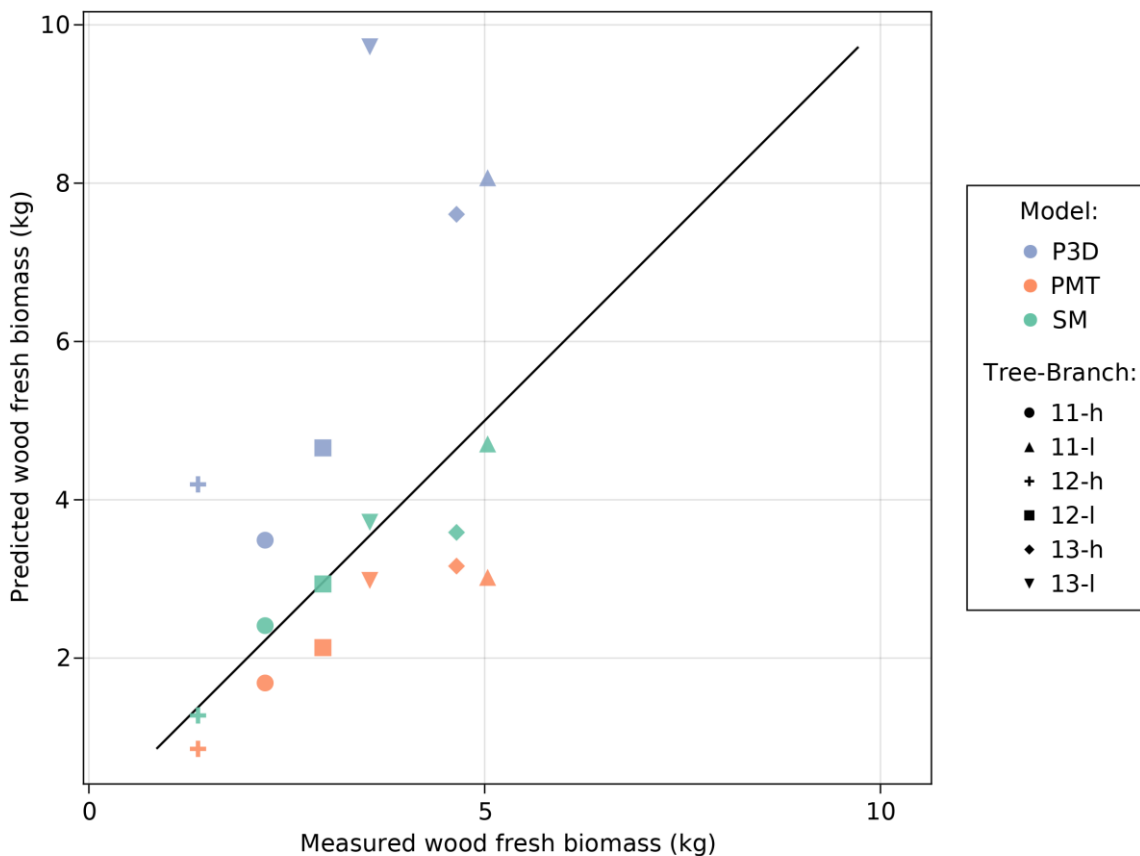
219 The structural model presented the lowest error for the prediction of the segments' CSA
 220 compared to the standard PMT, especially for the lower branch of tree 11 (11-l) that was
 221 systematically overestimated by the PMT (Figure 4). The structural model predicted the
 222 segments' CSA with higher accuracy than the PMT for all computed statistics; with an nRMSE
 223 half as high and a bias five times lower (Table 2).

224 **Table 2. Prediction accuracy of the models related to Figure 4 (n = 3461 each). RMSE: Root Mean Squared**
 225 **Error, nRMSE: normalized RMSE, EF: Modelling Efficiency, nBias: normalized bias. Best statistics are**
 226 **highlighted in bold. PMT: Pipe Model Theory, SM: Structural Model (this study).**

Model	RMSE	nRMSE	EF	Bias	nBias
PMT	103.3	0.02	0.95	17.92	0.0035
SM	57.7	0.01	0.98	2.89	0.0007

227 **3.3. Model evaluation with destructive measurements**

228 The model was evaluated using destructive measurements of the branches' woody biomass with
 229 a scale. The average point distance algorithm from Plantscan3d lead to a poor estimation of
 230 branch biomass with a systematic overestimation, an nRMSE of 92% (+3.38 kg) and an nBias of
 231 82% (2.99 kg, Table 3). The PMT improved the estimation with only 31% nRMSE but
 232 systematically underestimated the biomass by 27%, which represented *c.a.* -1 kg in average.



233

234 **Figure 5. Measured (x-axis) and predicted (y-axis) fresh wood biomass at branch scale. Branch scale is**
 235 **defined as the sum of the biomass of all manually identified axes to control for the error induced by missing**
 236 **structures between LiDAR scans and destructive measurements. P3D: Plantscan3d reconstruction using the**
 237 **average point distance algorithm; PMT: Pipe Model Theory; SM: Structural Model (this study). The branch is**
 238 **named after the tree index and the position in the tree: high (h) or low (l).**

239 The structural model however was the only model to present a modelling efficiency (EF) close to
 240 one, with a value of 0.87. It also presented a lower nRMSE of 13% and a bias closer to zero (-
 241 5%). The slight bias towards underestimation came from one branch in particular (-23%), the

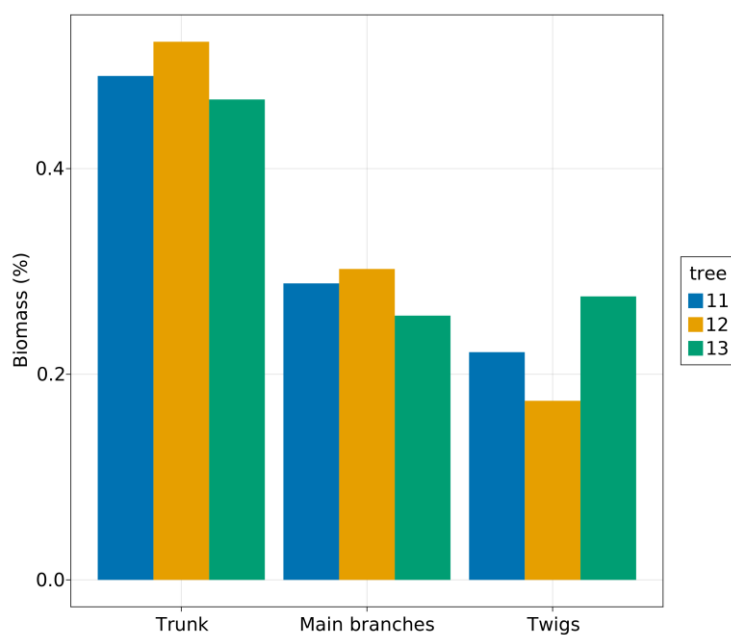
242 highest branch from tree 13 (13-h), that presented a high number of broken axes (35). The error
 243 was relatively higher for the finer structures though, with an error of 20% for structures below
 244 10 cm diameter.

245 **Table 3. Statistics about the model prediction of the fresh biomass at branch scale (n = 6, see Figure 5). RMSE:**
 246 **Root Mean Squared Error, nRMSE: normalized RMSE, EF: Modelling Efficiency, nBias: normalized bias. Best**
 247 **statistics are highlighted in bold. P3D: Plantscan3d; PMT: Pipe Model Theory; SM: Structural Model (this**
 248 **study).**

Model	RMSE	nRMSE	EF	Bias	nBias
P3D	3.38	0.92	-5.95	2.99	0.82
PMT	1.14	0.31	0.21	-0.99	-0.27
SM	0.47	0.13	0.87	-0.19	-0.05

249 3.4. Model application

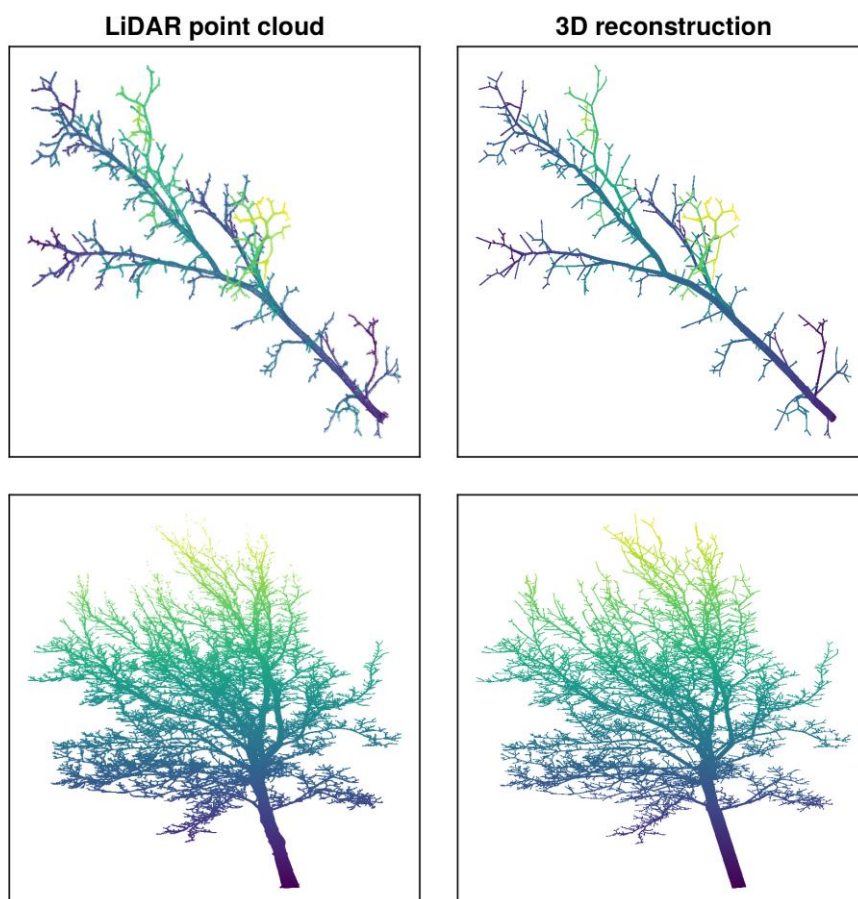
250 The structural model was applied at the whole tree level over the three walnut trees. The
 251 distribution of the aboveground woody biomass was similar between trees according to the
 252 three supervised classes of segment diameter. The trunk represented in average 50% of the
 253 biomass, the main branches 29%, and the twigs 21% (Figure 6). The total length of the
 254 structures in the tree represented in average 1735 m, with 96% of that length coming from the
 255 twigs.



256

257 **Figure 6. Relative distribution of the aboveground woody biomass estimated by the structural model for each**
258 **segment diameter class in the three walnut trees. Twigs: [0, 5); Main branches: [5, 15); Trunk: [15, 50) cm.**

259 Overall, the coupling of LiDAR point clouds, Plantscan3d skeletonization and the structural
260 model lead to precise 3D reconstructions of the targeted branches and the whole trees (Figure
261 7). At the branch level, even the smallest structures were satisfactorily reconstructed by the
262 skeletonization, and connection paths were correct despite the complexity of some structures. At
263 tree scale, the trunk base reconstruction was not completely visually realistic because it only
264 used one segment, but its estimated volume was probably close to reality. The estimated
265 topology of the structures in the tree was also close to observations at this scale, which is
266 particularly surprising considering there were no parameter except the number of nodes, and no
267 manual corrections applied after the fully automatic reconstruction of the branch and tree.



268

269 **Figure 7. Co-registered LiDAR point-cloud (left panels) and 3D reconstruction using the structural model**
270 **(right panels) of a sampled branch (top panels, 11-h) and a whole tree (bottom panels, 12). Note that the 3D**
271 **reconstruction was done at the segment level, which implies that the trunk base has only one segment.**

272 **4. Discussion**

273 Our first assumption was that we could improve on the method developed by Hu et al. (2021) by
274 using the full extent of the LiDAR data for the estimation of the aerial woody biomass. It was
275 based on the hypothesis that Plantscan3d was able to provide a correct estimation of the
276 topology and length of all structures in the tree, including finer branches. Our results validated
277 this assumption, showing that axis length estimations were close to the destructive
278 measurements across the whole range of sizes with almost zero bias (0.2%), which is important
279 when scaling-up to the tree or plot scale.

280 The main objective of this study was to design, train and evaluate a new approach for a more
281 precise estimation of the aboveground woody biomass. As expected, our results showed that
282 using the traditional approach of fitting the LiDAR point cloud to estimate the diameter of the
283 structures gave unsatisfactory predictions of the biomass with a systematic overestimation
284 (nRMSE: 92%, Figure 5, Table 3). This error can be explained by the noise in the point cloud
285 induced by the significant footprint of the laser or the movements of the branches from wind
286 and due to occlusion that lead to an insufficient sampling of some structures.

287 The PMT, another standard method that only rely on the topology and diameter estimated at the
288 base, was also tested and gave acceptable results with an nRMSE of 31% and a bias of -27%. The
289 results are particularly impressive giving that no parameters were used for this method except
290 for the diameter at the base and the number of nodes from base to main axis tip. We propose
291 that this model should be used in a first approximation of the biomass when no further data is
292 available.

293 The new method presented in this paper showed that including structural-based knowledge to
294 the modelling process significantly improved the estimation of the diameters. The structural

295 model predicted segments diameters with only 1% nRMSE, and gave satisfactory results when
296 applied to the branch scale for the prediction of the woody biomass, with a significantly lower
297 error (13% nRMSE) and bias (-5%) compared to the other methods. Furthermore, the error was
298 primarily driven by one branch (13-h) and was already observed on the prediction of the cross
299 section (Figure 4) of one of the widest axis for both the PMT and the structural model. Knowing
300 the process of estimation of both models, this indicates that the error most probably came from
301 the high number of broken structures in this branch, which hinders a proper estimation due to a
302 loss of information about the variables used in the model, and most notably the number of
303 terminal segments and the total length of the subtree.

304 For comparison, Calders et al. (2015) reported whole-tree nRMSE of 16.1% and 9.68% nBias
305 using TreeQSM. Kunz et al. (2017) measured whole tree volumes and used TreeQSM for the
306 reconstruction with average nRMSE of 22.7% and 6% nBias, and Burt et al. (2021) showed only
307 2.8% relative error using TreeQSM on whole trees. It is important to note that those reported
308 errors would most probably be higher if reported only for the twigs as they are in this study,
309 because most of the error comes from structures with lower diameters, which represented 21%
310 of the total biomass in this study. Demol et al. (2022) showed for example that 80-83% of the
311 bias from their whole-tree reconstruction originated from the structures with a diameter lower
312 than five centimeters, and the structures below or equal 10 cm diameter had errors of *c.a.* 139%,
313 when we report errors of only 20% with our method.

314 The structural model allowed for a better estimation of the branches biomass with very little
315 bias, which is required for computations at the tree or plot level. However, it requires data for
316 training, unlike the simple PMT or the biased mean point distance algorithm. In our study, two
317 people were able to measure one branch per day, including cutting, measuring biomass of the
318 whole branch and of the secondary axis, full topology, and segments diameter and length. The
319 model is trained once, and can be applied without further parameterization. This is particularly

320 true when considering that Plantscan3d does not require any complex parameters to
321 reconstruct tree topology and spatial arrangement. This allows for fast estimations of the
322 aboveground woody biomass at larger scale, or repeated estimations for the monitoring of
323 growth and development.

324 One of the most interesting result of this study is how the structural model is generic enough to
325 predict the cross-sectional area of all structures in the tree, although trained only over two
326 branches per tree. The application of the structural model to the whole tree showed that
327 structures with a diameter lower than 5 cm represented 22% of the tree aerial woody biomass.
328 These results indicate that a substantial portion of the biomass can be lost if not properly used
329 or handled.

330 The 3D reconstruction of the trunk base at tree-level is slightly unrealistic because only one
331 segment was used. This issue can be easily corrected using the mean point distance algorithm
332 from Plantscan3d for the structures with largest diameters instead. These bigger structures are
333 not prone to the issues presented in this paper, so algorithms using the LiDAR point cloud to
334 compute the diameters should be sufficient. The quality of the whole-tree reconstruction shows
335 that the skeletonization algorithm from Plantscan3d is highly suitable for this task, especially
336 considering that it only uses one parameter (*i.e.* the total number of nodes between the base and
337 the tip of the main axis) on which it has little sensitivity. For comparison, TreeQSM uses more
338 than twenty parameters, and its reconstructions were shown to be highly sensitive to the
339 parameter values (Demol et al., 2022).

340 The new method presented in this study is promising but need further applications on other
341 conditions. Further work may investigate the minimal and optimal set of data needed to define
342 and parameterize the architectural model giving an acceptable prediction error. The method
343 was also found sensitive to a high number of broken structures, which means that the estimation
344 of the aerial woody biomass of highly pruned trees must be done with caution, unless trained

345 specifically on such data. In any case, further improvements to the method should include a way
346 of accounting for pruned structures, by *e.g.* using the LiDAR-derived diameters as a first
347 approximation to identify where the structure deviate from the PMT, and mark those nodes as
348 potential pruning sites.

349 **5. Conclusion**

350 The Plantscan3d software was able to reconstruct the branches topology and axis lengths with
351 high accuracy. Visual evaluations showed it also performed correctly at the whole-tree level,
352 even for finer branches. Our results confirm that LiDAR point-clouds can be used for accurate
353 reconstructions of trees, except for the estimation of finer branches diameters.

354 In this study, we present a new method for the estimation of the diameters and woody biomass
355 of trees. It outperformed the two standard approaches of adjusting cylinders to the LiDAR point-
356 cloud or using the pipe model theory. The method is designed to use most of the information
357 extractable from the LiDAR point cloud, while controlling the effect of under-sampling (*i.e.*
358 occlusions), light winds or laser footprint. The structural model was applied at the whole-tree
359 level, and showed that 96% of the length and 21% of the biomass were located in the finer
360 branches with a diameter lower than 5 cm. These results indicate that most of the studies that
361 do not account for finer branches could miss a substantial part of the biomass in the trees.

362 The structural model approach could pave the way for a better assessment of whole-tree
363 aboveground woody biomass using LiDAR, with very low need for destructive sampling for
364 model training and validation, while controlling errors induced by wind, low sampling and laser
365 footprint.

366 **Conflicts of interest**

367 None.

368 **Acknowledgements**

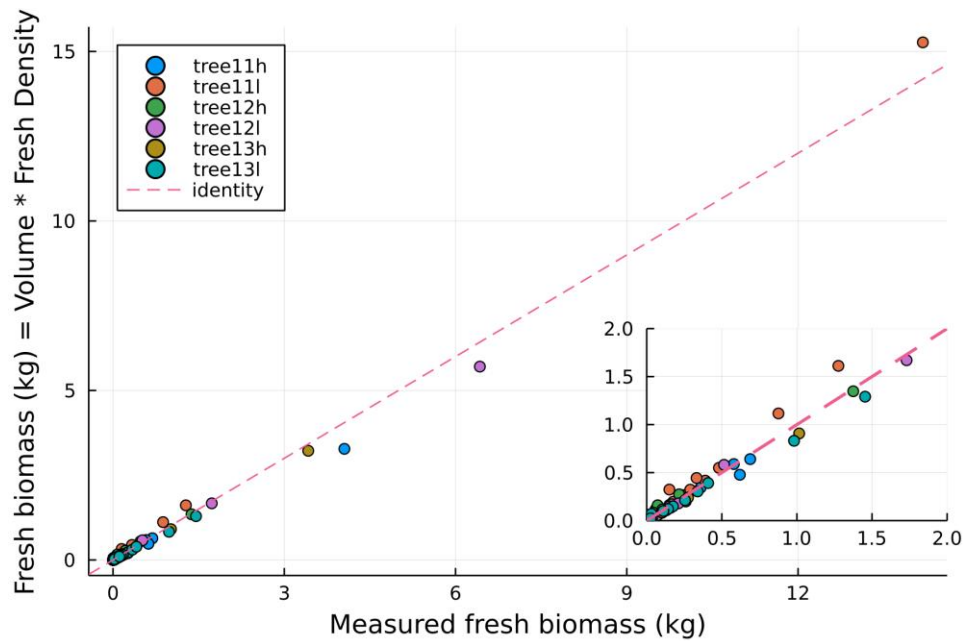
369 This research was supported by the French « Agence de l'environnement et de la maîtrise de
370 l'énergie » (ADEME) in the framework of the AGROBRANCHE (Study of the branches valorisation
371 in agroforestry for bio-based materials and chemistry sectors) project from 2018 to 2022. We
372 thank the experimentation team from the AMAP lab for their support: Stéphane Fourtier
373 (INRAE), Merlin Ramel (INRAE), Sophie Nourissier-Mountou (CIRAD), Chantal Geniez (IRD) and
374 Quentin Le Blaye (INRAE).

375 **Authors' Contributions**

376 RV and MM wrote the manuscript, MM, AB, JD and RV did the field work with the
377 experimentation team, JD and RV made the LiDAR scans with the help of Merlin Ramel, RV
378 developed the code, trained the models and made the visualizations, RV, MM, AB, and JD
379 analysed the results.

380 **Appendix A**

381 The estimation of the woody biomass from the structural model used the dimensions of the
382 segments and an average wood density. The error coming from this estimation can be computed
383 using only the destructive measurements. We can compare the reference fresh biomass
384 measured using a scale with the biomass estimated from the average fresh wood density and the
385 volume computed from the segment dimensions (*i.e.* diameter and length) measured by hand.



386

387 **Figure A 1.** Fresh biomass measured with a scale on the field (x) compared to its calculation using an average
 388 branch fresh wood density and segment volume estimated with the segment's radius and length (y). Each
 389 point is an axis on the branch. First order axis biomass is defined as the sum of its segments biomass,
 390 excluding higher order axis, and second order axis biomass is defined as the sum of all segments it bears.
 391 RMSE: 105.81g, nRMSE: 1%, EF: 0.99.

392 The results show that the computed axis biomass from its volume and an average wood fresh
 393 density was close to the scale measurement, with a low nRMSE of 1% and a modelling efficiency
 394 close to one.

395 References

396 Abegg, M., Boesch, R., Schaepman, M.E., Morsdorf, F., 2021. Impact of Beam Diameter and
 397 Scanning Approach on Point Cloud Quality of Terrestrial Laser Scanning in Forests. *IEEE*
 398 *Transactions on Geoscience and Remote Sensing* 59, 8153–8167.
 399 <https://doi.org/10.1109/TGRS.2020.3037763>

400 Boudon, F., Preuksakarn, C., Ferraro, P., Diener, J., Nacry, P., Nikinmaa, E., Godin, C., 2014.
 401 Quantitative assessment of automatic reconstructions of branching systems obtained
 402 from laser scanning. *Annals of Botany* 114, 853–862.
 403 <https://doi.org/10.1093/aob/mcu062>

404 Burt, A., Boni Vicari, M., da Costa, A.C.L., Coughlin, I., Meir, P., Rowland, L., Disney, M., 2021. New
 405 insights into large tropical tree mass and structure from direct harvest and terrestrial
 406 lidar. *Royal Society Open Science* 8, 201458. <https://doi.org/10.1098/rsos.201458>

407 Calders, K., Adams, J., Armston, J., Bartholomeus, H., Bauwens, S., Bentley, L.P., Chave, J., Danson,
 408 F.M., Demol, M., Disney, M., Gaulton, R., Krishna Moorthy, S.M., Levick, S.R., Saarinen, N.,
 409 Schaaf, C., Stovall, A., Terry, L., Wilkes, P., Verbeeck, H., 2020. Terrestrial laser scanning
 410 in forest ecology: Expanding the horizon. *Remote Sensing of Environment* 251, 112102.
 411 <https://doi.org/10.1016/j.rse.2020.112102>

- 412 Calders, K., Newnham, G., Burt, A., Murphy, S., Raumonen, P., Herold, M., Culvenor, D., Avitabile,
413 V., Disney, M., Armston, J., Kaasalainen, M., 2015. Nondestructive estimates of above-
414 ground biomass using terrestrial laser scanning. *Methods in Ecology and Evolution* 6,
415 198–208. <https://doi.org/10.1111/2041-210X.12301>
- 416 Dassot, M., Constant, T., Fournier, M., 2011. The use of terrestrial LiDAR technology in forest
417 science: application fields, benefits and challenges. *Annals of Forest Science* 68, 959–974.
418 <https://doi.org/10.1007/s13595-011-0102-2>
- 419 Demol, M., Wilkes, P., Raumonen, P., Krishna Moorthy, S.M., Calders, K., Gielen, B., Verbeeck, H.,
420 2022. Volumetric overestimation of small branches in 3D reconstructions of *Fraxinus*
421 *excelsior*. *Silva Fennica* 56.
- 422 Godin, C., Caraglio, Y., 1998. A Multiscale Model of Plant Topological Structures. *Journal of*
423 *Theoretical Biology* 191, 1–46. <https://doi.org/10.1006/jtbi.1997.0561>
- 424 Hu, M., Pitkänen, T.P., Minunno, F., Tian, X., Lehtonen, A., Mäkelä, A., 2021. A new method to
425 estimate branch biomass from terrestrial laser scanning data by bridging tree structure
426 models. *Annals of Botany* 128, 737–752. <https://doi.org/10.1093/aob/mcab037>
- 427 Kunz, M., Hess, C., Raumonen, P., Bienert, A., Hackenberg, J., Maas, H.-G., Härdtle, W., Fichtner, A.,
428 Von Oheimb, G., 2017. Comparison of wood volume estimates of young trees from
429 terrestrial laser scan data. *iForest - Biogeosciences and Forestry* 10, 451.
430 <https://doi.org/10.3832/ifer2151-010>
- 431 Lehnebach, R., Beyer, R., Letort, V., Heuret, P., 2018. The pipe model theory half a century on: a
432 review. *Annals of Botany* 121, 773–795. <https://doi.org/10.1093/aob/mcx194>
- 433 Perez, R.P.A., Costes, E., Theveny, F., Griffon, S., Caliman, J.-P., Dauzat, J., 2018. 3D plant model
434 assessed by terrestrial LiDAR and hemispherical photographs: A useful tool for
435 comparing light interception among oil palm progenies. *Agricultural and Forest*
436 *Meteorology* 249, 250–263. <https://doi.org/10.1016/j.agrformet.2017.11.008>
- 437 Raumonen, P., Kaasalainen, M., Åkerblom, M., Kaasalainen, S., Kaartinen, H., Vastaranta, M.,
438 Holopainen, M., Disney, M., Lewis, P., 2013. Fast Automatic Precision Tree Models from
439 Terrestrial Laser Scanner Data. *Remote Sensing* 5, 491–520.
440 <https://doi.org/10.3390/rs5020491>
- 441 Shinozaki, K., Yoda, K., Hozumi, K., Kira, T., 1964. A quantitative analysis of plant form-the pipe
442 model theory: I. Basic analyses. *Japanese Journal of ecology* 14, 97–105.
- 443 Thies, M., Pfeifer, N., Winterhalder, D., Gorte, B.G., 2004. Three-dimensional reconstruction of
444 stems for assessment of taper, sweep and lean based on laser scanning of standing trees.
445 *Scandinavian Journal of Forest Research* 19, 571–581.
- 446 Valentine, H.T., 1985. Tree-growth models: derivations employing the pipe-model theory.
447 *Journal of theoretical biology* 117, 579–585.
- 448 Vezy, R., 2022. MultiScaleTreeGraph.jl: Read, write, analyze, compute and plot multi-scale tree
449 graph files. <https://doi.org/10.5281/zenodo.7004348>
- 450 Vezy, R., Millan, M., Bonnet, A., Dauzat, J., 2022. Data and code for the article “Coupling LiDAR and
451 structural models to improve the estimation of aboveground woody biomass.”
452 <https://doi.org/10.5281/zenodo.7038482>
- 453 Wilkes, P., Lau, A., Disney, M., Calders, K., Burt, A., Gonzalez de Tanago, J., Bartholomeus, H.,
454 Brede, B., Herold, M., 2017. Data acquisition considerations for Terrestrial Laser

455 Scanning of forest plots. *Remote Sensing of Environment* 196, 140–153.
456 <https://doi.org/10.1016/j.rse.2017.04.030>

457 Wilkes, P., Shenkin, A., Disney, M., Malhi, Y., Bentley, L.P., Vicari, M.B., 2021. Terrestrial laser
458 scanning to reconstruct branch architecture from harvested branches. *Methods in*
459 *Ecology and Evolution* 12, 2487–2500. <https://doi.org/10.1111/2041-210X.13709>

460 Xu, H., Gossett, N., Chen, B., 2007. Knowledge and heuristic-based modeling of laser-scanned
461 trees. *ACM Transactions on Graphics (TOG)* 26, 19-es.

462